IEEE Photonics Journal
An IEEE Photonics Society Publication

Open Access

Preliminary Characterization of Coverage for Water-to-Air Visible Light Communication Through Wavy Water Surface

Volume 13, Number 1, February 2021

Tianrui Lin
Nuo Huang
Chen Gong, *Senior Member, IEEE*
Jianghua Luo
Zhengyuan Xu, *Senior Member, IEEE*

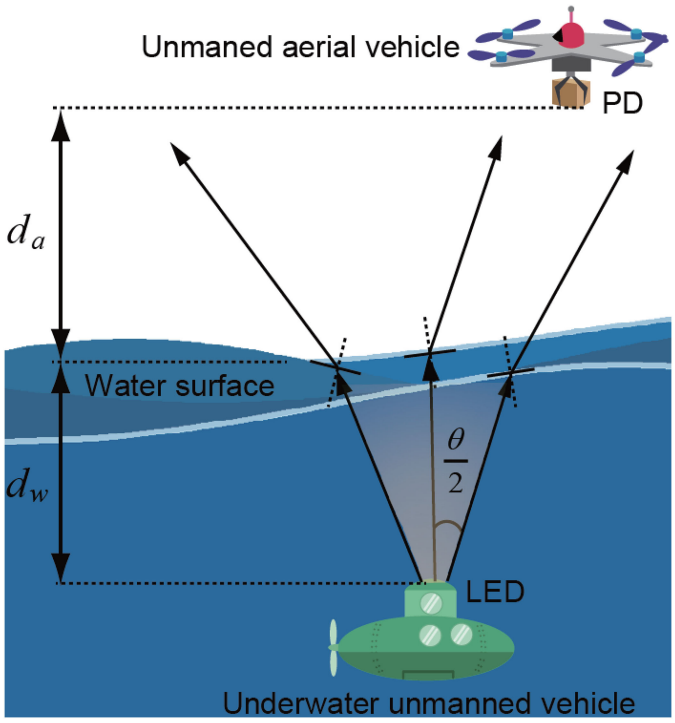

DOI: 10.1109/JPHOT.2021.3054911

Preliminary Characterization of Coverage for Water-to-Air Visible Light Communication Through Wavy Water Surface

Tianrui Lin,[1] Nuo Huang ,[1] Chen Gong ,[1] *Senior Member, IEEE*, Jianghua Luo,[2,3] and Zhengyuan Xu ,[1] *Senior Member, IEEE*

[1]Key Laboratory of Wireless-Optical Communications, Chinese Academy of Sciences, School of Information Science and Technology, University of Science and Technology of China, Hefei 230027, China
[2]School of Physics and Optoelectronic Engineering, Yangtze University, Jingzhou 434023, China
[3]Zhongshan Zhongchuang Technology Research Institute of Opto-Electronics Industry, Zhongshan 528415, China

DOI:10.1109/JPHOT.2021.3054911

Manuscript received January 4, 2021; revised January 21, 2021; accepted January 22, 2021. Date of publication January 28, 2021; date of current version February 12, 2021. This work was supported in part by National Key Research and Development Program of China under Grant 2018YFB1801904, in part by the National Postdoctoral Program for Innovative Talents under Grant BX20190320, in part by the project funded by China Postdoctoral Science Foundation under Grant 2020M671896, in part by Key Program of National Natural Science Foundation of China under Grant 61631018, in part by Key Research Program of Frontier Sciences of CAS under Grant QYZDY-SSW-JSC003, and in part by the open research fund of National Mobile Communications Research Laboratory Southeast University under Grant 2019D14. Corresponding authors: Nuo Huang; Chen Gong (e-mail: huangnuo@ustc.edu.cn; cgong821@ustc.edu.cn).

Abstract: In this paper, we establish a water-to-air (W2A) visible light communication (VLC) link using green light emitting diode (LED), and investigate the coverage characteristics of the designed W2A-VLC link under calm and wavy water conditions. By transmitting a high-frequency sinusoid signal, we extract the variation of link gain. Based on the received signals of an experimental W2A-VLC system, we obtain the real link gains at different receiver points and analyze the channel temporal properties in good link conditions (called link "on" state). It is seen that the mean channel gain under wavy water surface condition can be larger than that under calm water surface condition, especially when the transmitter and receiver are not perfectly aligned, due to the random spatial modulation effect of wavy water surface. Moreover, the "on" state duration and interval can be well fitted by a shifted exponential distribution and a shifted lognormal distribution, respectively. Bit error rate (BER) results reveal the effect of expanded link gain variation under wavy water surface condition. This work provides significant guidance for future works on the communication protocol design and related performance analysis.

Index Terms: Coverage characterization, visible light communication, water-to-air communication, wavy water surface.

1. Introduction

In recent years, underwater activities and related wireless communication have drawn great interest from both academia and industry [1]–[3]. To explore and acquire data from ocean efficiently

and safely, it is essential to establish communication links between underwater platforms (e.g., underwater unmanned vehicle (UUV) and sensors) and terrestrial platforms (e.g., unmanned aerial vehicle (UAV) and base stations) [4]–[6]. Reliable communication across the water-to-air (W2A) interface plays an important role in various applications such as underwater monitoring and underwater rescue missions [7].

Radio frequency wave (RF), acoustic wave and optical wave are three existing wireless carriers for transmission in the air and water. Although RF signal can travel a long distance (up to tens of kilometers) and achieve a high transmission rate (up to hundreds of Mbps) in the air, they can only propagate few meters through water due to high absorption and attenuation [8]. Acoustic wave can travel several kilometers in the water and has been the prime choice for underwater communication. However, the transmission rate of an acoustic communication system is only in the order of kilo bits per second, which cannot reach the requirements of potential applications. Besides, acoustic wave will be mostly reflected off the water surface and it suffers high attenuation in the air [9]. To sum up, neither RF nor acoustic wave can be used alone for communication across the W2A interface. Noting that the transmission characteristics of RF and acoustic waves can be complementary in different media, one straightforward solution is to combine the two methods, which yields translational acoustic-RF communication (TARF) [10]. In a TARF system, acoustic signal travels as pressure waves causing displacements of the water surface. An airborne radar can monitor and decode these surface perturbations. Although such system can operate under waves below 16 cm, the transmission rate is limited to 400 bps at the cost of high hardware complexity.

The recent advance in optical wireless communication (OWC) promotes the consideration of optical wave as an alternative for communication across the W2A interface. It has been demonstrated that water exhibits an acceptable attenuation for light in the blue-green window (from 450 nm to 550 nm), laying the foundation of underwater optical wireless communication [11]. Compared with RF and acoustic waves, optical wave possesses several distinct advantages. Firstly, the propagation attenuation of optical wave is acceptable in both water and air medium. Secondly, according to Fresnel formula, most of the light energy can pass through the W2A interface for small-to-medium incident angle. Thirdly, OWC can provide high transmission rate at relatively low cost. These appealing features make OWC one promising technology for communication across the W2A interface [12].

Over the past years, some studies have been carried out for W2A-OWC, mainly including channel characterization and system realization. In [13], the statistics of W2A-OWC channel impulse response under different water surface conditions were fitted by typical probabilistic distributions. In [14], the link gain and delay of W2A-OWC were evaluated using Monte Carlo simulations to show the influence of dynamic environment. A feedback-assisted orbital angular momentum-based W2A-OWC link was established in [15], using a 520 nm green light laser diode. In [16], an ultraviolet communication system was demonstrated across the wavy W2A interface. A W2A laser communication system was realized in [17], which achieves a data rate of 44 Mb/s over a 2.3-m underwater and 3.5-m air link. Furthermore, different multi-carrier W2A laser communication systems were developed in [18] and [19] to alleviate the fading effect.

In real communication scenarios, wavy surface may randomly change the direction of light propagating into the air, which has not been addressed in [15] and [18]. The transmitter and receiver may fluctuate with the environments and not be perfectly aligned in practical W2A-OWC scenarios, which has not been addressed in [13], [15]–[19]. For robust transmission design in real W2A environments, it is essential to characterize the coverage of the W2A-OWC system by investigating the link characteristics at different receiver points. Although coverage characteristics were investigated in [14], the results are only based on computer simulations and lack experimental demonstration.

To address the above issues, in this work, we establish a W2A visible light communication (VLC) link using green light emitting diode (LED) and experimentally investigate the coverage characteristics of the W2A link under calm and wavy water surface conditions. Using a high-frequency sinusoid signal, we extract the variation of link gain. By collecting the received signals of an experimental

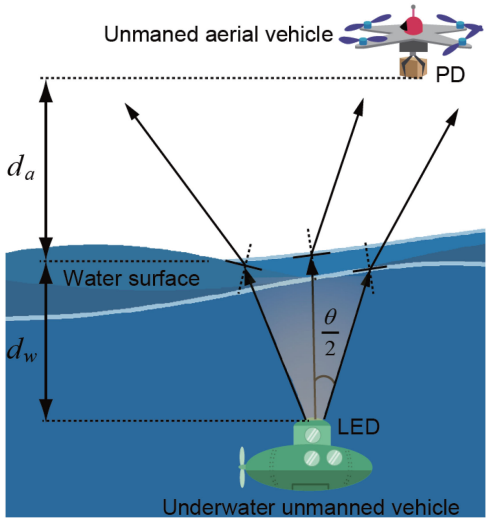

Fig. 1. Illustration of the considered W2A-VLC scenario.

W2A-VLC system, we obtain the real link gains at different receiver points and analyze the channel temporal properties in good link conditions (or called link "on" state in the remainder of this paper). It is seen that the mean channel gain through wavy water surface can be larger than that through calm water surface, especially when the transmitter and receiver are not perfectly aligned, due to the random spatial modulation effect of wavy water surface. Moreover, the "on" state duration and interval can be well fitted by a shifted exponential distribution and a shifted lognormal distribution, respectively. Bit error rate (BER) results reveal the effect of expanded link gain variation under wavy water surface condition. Against the current research works, this work investigates the coverage characteristics for W2A-OWC link via real experiments. The results can provide significant guidance for future works on the communication protocol design and related performance analysis.

The remainder of this paper is organized as follows. Section II describes the system model. The signal processing approach is presented in Section III. The experimental setup is elaborated in Section IV. The experimental results are presented and analyzed in Section V. Finally, Section VI concludes this paper.

2. System Descriptions

Consider a W2A-VLC scenario where one UUV conveys information to one UAV, as shown in Fig. 1. The UUV is equipped with one green/blue LED transmitter at depth d_w under the water. The UAV is equipped with one photodiode (PD) (e.g., avalanche photodiode (APD)) receiver at height d_a above the water surface. The LED with beam angle θ transmits the modulated optical signal to the PD. The light first propagates in the water and then is refracted at the water surface. As the water has a larger refractive index than the air, the refraction angle is larger than the incident angle. After penetrating into the air, the light is detected by the PD receiver for further signal processing.

Under a calm water surface condition, the received light spot is circular at fixed height in the air. However, due to the wind and tide effects, the water surface is not completely flat in practical scenarios. As a consequence, the received light spot is irregularly shaped, which implies that the received signal strength at a fixed receiver position varies with time. The dynamic variation of light spot is promising because it boosts the coverage area such that the communication link still remains effective even when the transmitter and receiver are not perfectly aligned. To facilitate the transmission design for a W2A-VLC system, it is essential to investigate the coverage characteristics by analyzing the link gain variations at different receiver points.

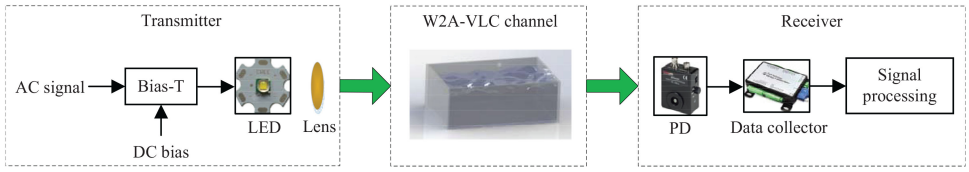

Fig. 2. The block diagram of a laboratory W2A-VLC system.

3. Signal Processing

The block diagram of a laboratory W2A-VLC system is shown in Fig. 2. The system consists of the transmitter part, the W2A link and the receiver part. At the transmitter, the direct current (DC) and alternating current (AC) signals are combined by a bias-tee circuit to drive the LED. The modulated visible light reaches the PD receiver through the W2A-VLC link. At the receiver, the PD detects the optical signal and converts it into the electrical signal, which is collected by a data collector for further processing.

We only consider the LOS (line-of-sight) link between the transmitter and receiver, since it is the dominant path in the W2A-VLC system. Then, the received signal at time t can be expressed as

$$y(t) = r(t) \otimes [h(t) \cdot x(t)] + z(t), \tag{1}$$

where $x(t)$ denotes the transmitted optical signal, $h(t)$ denotes the LOS W2A-VLC channel gain, $r(t)$ denotes the impulse response of the PD, $z(t)$ denotes the additive noise, and $\otimes$ denotes the convolution operation. For calm water surface, the channel gain $h(t)$ can be considered as a constant, i.e., $h(t) = h_c$. In contrast, $h(t)$ varies with time for wavy water surface. Denote the frequency of wavy water surface by f_w. The dominant frequency band of $h(t)$ is $[-f_w, f_w]$ for wavy water surface. Typically, f_w is less than 100 Hz.

One intuitionistic idea on recording the channel variation is to transmit a constant DC signal $x(t) = d$ and measure the received signal strength for calm and wavy water surface conditions. Note that the PD has a low-frequency cutoff property, as seen from Fig. 3(a). With $x(t) = d$, signal $h(t)x(t)$ has a near DC frequency under calm water surface condition while it has a main lobe $[-f_w, f_w]$ under wavy water surface condition, as shown in Fig. 3(b). In this case, the frequency response of PD to signal $h(t)x(t)$ under calm water surface condition is lower than that under wavy water surface condition. As a consequence, the channel gain comparison under calm and wavy water surface conditions cannot be directly obtained from the received signal strength corresponding to the transmitted DC signal.

To address the above issue, we transmit a sinusoid signal with a high frequency $f_c \gg f_w$, i.e., $x(t) = d + A\sin(2\pi f_c t + \varphi)$, where d is the DC bias for driving the LED, $f_c \in [f_L, f_H]$, and $[f_L, f_H]$ is the passband of the PD. Signal $Ah(t)\sin(2\pi f_c t + \varphi)$ has a frequency about f_c under calm water surface condition while it has a main lobe $[f_c - f_w, f_c + f_w]$ under wavy water surface condition, as shown in Fig. 3(c). Since $f_c \gg f_w$, the frequency response of the PD can be considered as a constant (denoted by R) in narrow band $[f_c - f_w, f_c + f_w]$. Using this fact, we propose one method to extract the variation of $h(t)$ from the received signal $y(t)$.

With $x(t) = d + A\sin(2\pi f_c t + \varphi)$, the received signal ignoring the noise is given by

$$y(t) = r(t) \otimes [dh(t) + Ah(t)\sin(2\pi f_c t + \varphi)]. \tag{2}$$

Through a high-pass filter, we can remove the components $r(t) \otimes [dh(t)]$ in $y(t)$ to obtain the signal

$$y_1(t) = RAh(t)\sin(2\pi f_c t + \varphi), \tag{3}$$

where R denotes the approximately constant frequency response of the PD in narrow band $[f_c - f_w, f_c + f_w]$. The square of $y_1(t)$ can be expressed as

$$\begin{aligned} y_2(t) &= y_1^2(t) \\ &= R^2A^2h^2(t)\sin^2(2\pi f_c t + \varphi) \end{aligned}$$

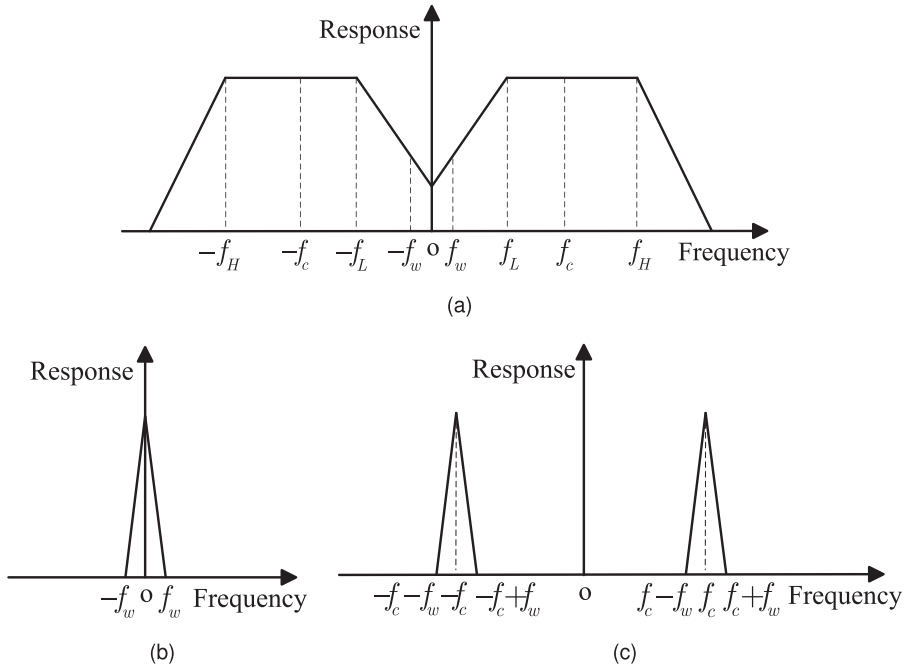

Fig. 3. Frequency response of relevant signals. (a) $r(t)$. (b) $dh(t)$ for wavy water surface. (c) $Ah(t)\sin(2\pi f_c t+\varphi)$ for wavy water surface.

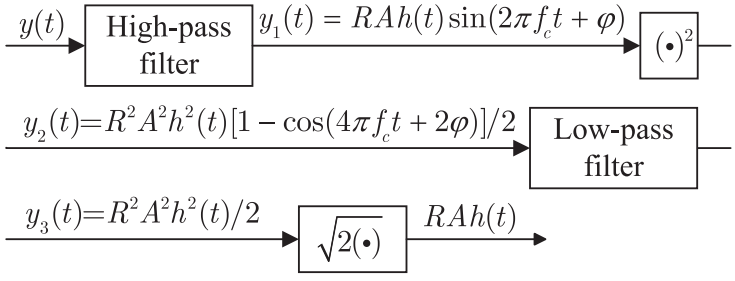

Fig. 4. Overall procedure for extracting the variation of $h(t)$.

$$= \frac{R^2A^2h^2(t)[1-\cos(4\pi f_c t+2\varphi)]}{2}. \tag{4}$$

Equation (4) implies that signal $y_2(t)$ contains DC component $\frac{R^2A^2h^2(t)}{2}$ and AC component $\frac{-R^2A^2h^2(t)[\cos(4\pi f_c t+2\varphi)]}{2}$. AC component $\frac{-R^2A^2h^2(t)[\cos(4\pi f_c t+2\varphi)]}{2}$ can be removed by feeding $y_2(t)$ into a low-pass filter, yielding signal

$$y_3(t) = \frac{R^2A^2h^2(t)}{2}. \tag{5}$$

Finally, we can obtain the variation of $h(t)$ via the square root operation on $2y_3(t)$, i.e.,

$$\sqrt{2y_3(t)} = RAh(t) \propto h(t), \tag{6}$$

where $\propto$ means 'proportional to'. The overall procedure for extracting the variation of $h(t)$ is summarized in Fig. 4.

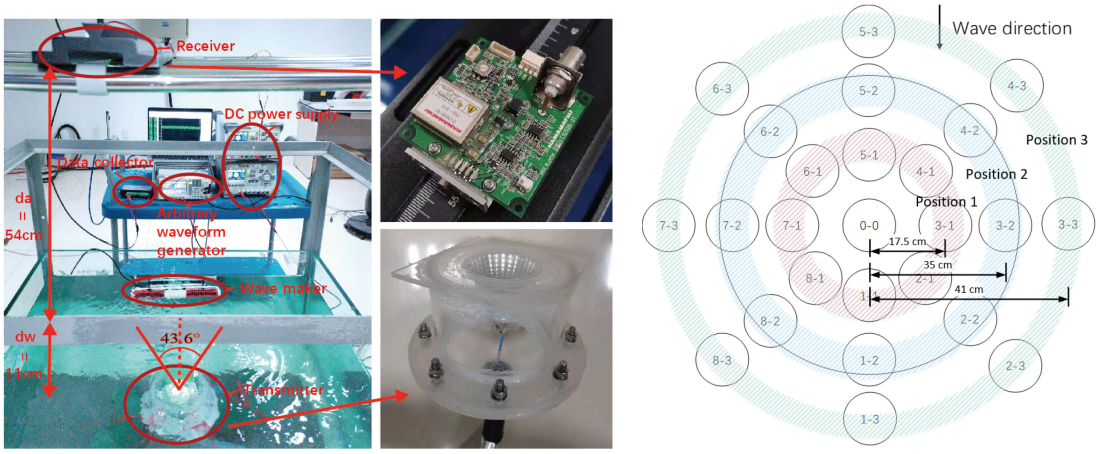

Fig. 5. The experimental environment. (a) The experimental W2A-VLC system. (b) Illustration of receiver points.

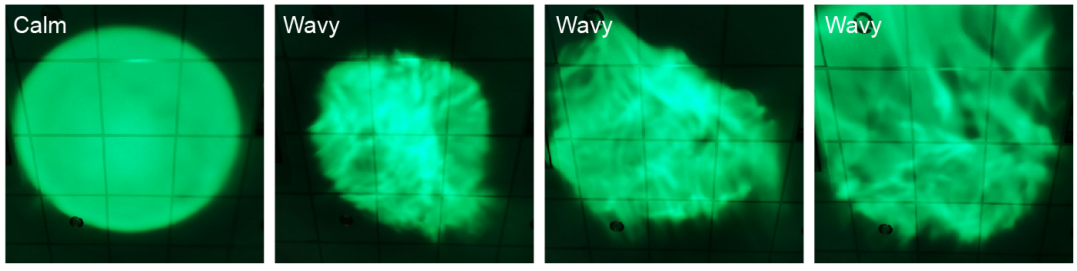

Fig. 6. The light spots under calm and wavy surface conditions.

4. Experimental Setup

To investigate the coverage characteristics of W2A link, we establish a W2A-VLC link and conduct preliminary experiment in the laboratory environment. Figure 5(a) shows the experimental W2A-VLC system. A green LED (Cree XBDGRN, 520 nm∼535 nm) is encapsulated in an acrylic container at depth 11 cm under the water surface (i.e., $d_w = 11$ cm). A lens with adjustable focus is placed in front of the LED to change the divergence angle of the beam. In the experiment, the beam angle is approximately 43.6°. The LED is driven by a bias-T combining the DC bias from a DC power supply (Rigol DP832 A) with sinusoidal wave (50 kHz, Vpp=2 V) from an arbitrary waveform generator (Rigol DG5252), through a waterproof cable attached to the end of the container. A wave maker is fixed to one side of the water tank for generating wavy surface to model the real sea environment. The light beam emitted from LED is then focused by the lens and passes through the acrylic plate into the water. Then, the beam propagates in the water and passes through the water surface.

The receiver end is located on a slide 54 cm above the water surface (i.e., $d_a = 54$ cm). Taking the center of the light spot as the origin, we set a total of 25 positions in eight directions symmetrically (shown in Fig. 5(b)), which includes three typical position relationships: APD aperture is inside (receiver point 0-0, at light spot center; position 1, 17.5 cm from light spot center), on the edge of (position 2, 35 cm from light spot center) or outside (position 3, 41 cm from light spot center) the light spot. An APD (Hamamatsu C10508-01) with an amplification circuit is used to convert the received optical signal to electrical signals. The outputs of APD are sampled by the data collector

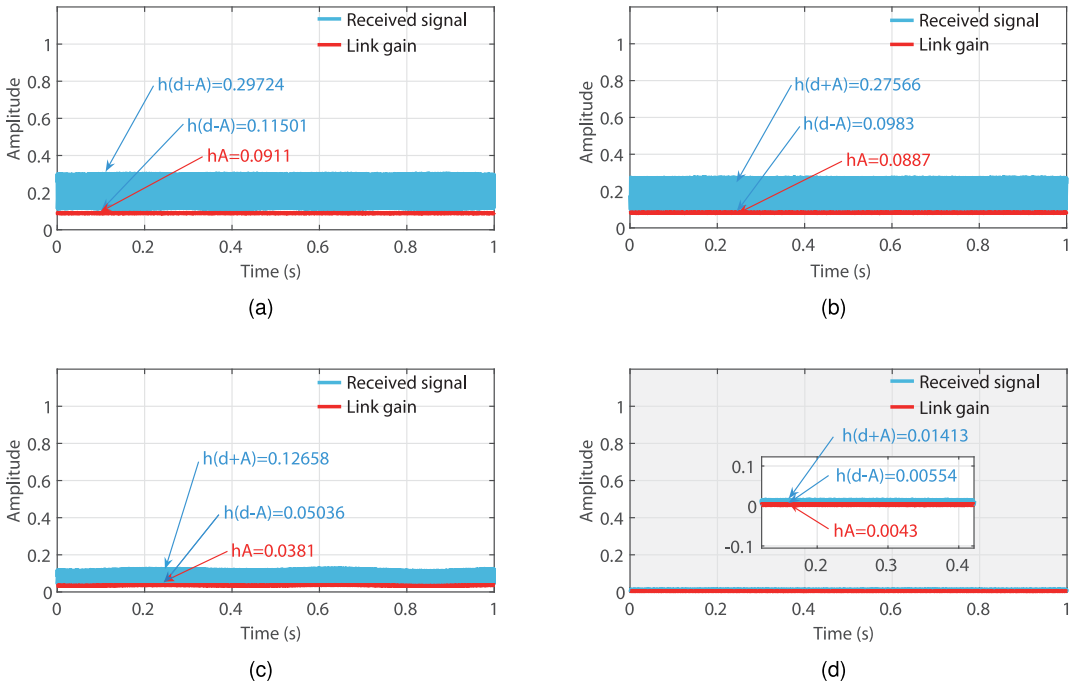

Fig. 7. The received signals and link gains in direction 8 under calm surface condition. (a) Receiver point 0-0. (b) Receiver point 8-1. (c) Receiver point 8-2. (d) Receiver point 8-3.

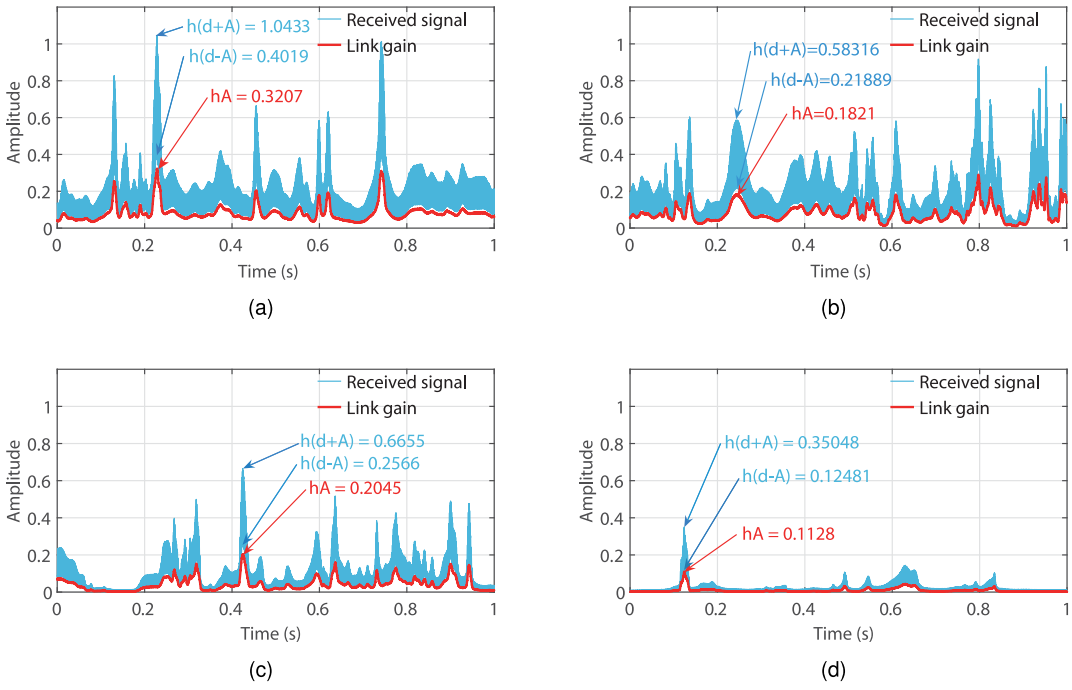

Fig. 8. The received signals and link gains in direction 8 under wavy surface condition. (a) Receiver point 0-0. (b) Receiver point 8-1. (c) Receiver point 8-2. (d) Receiver point 8-3.

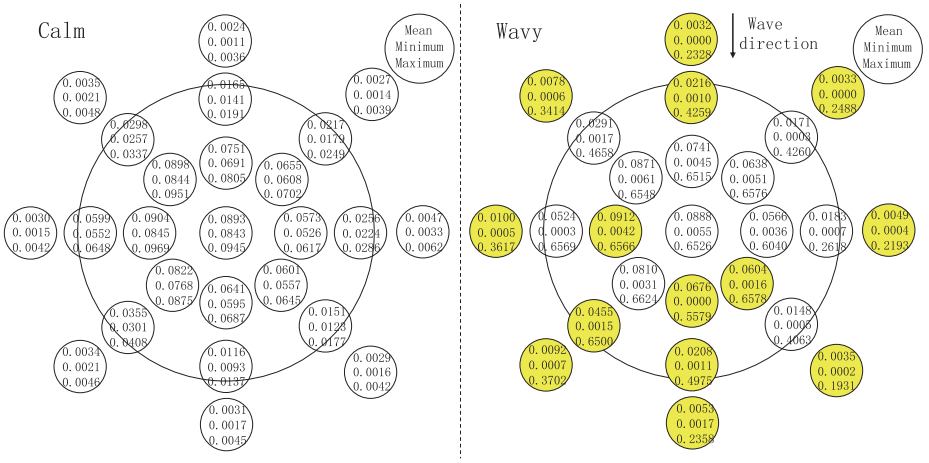

Fig. 9. Mean, minimum and maximum link gains at each receiver point under calm and wavy surface conditions.

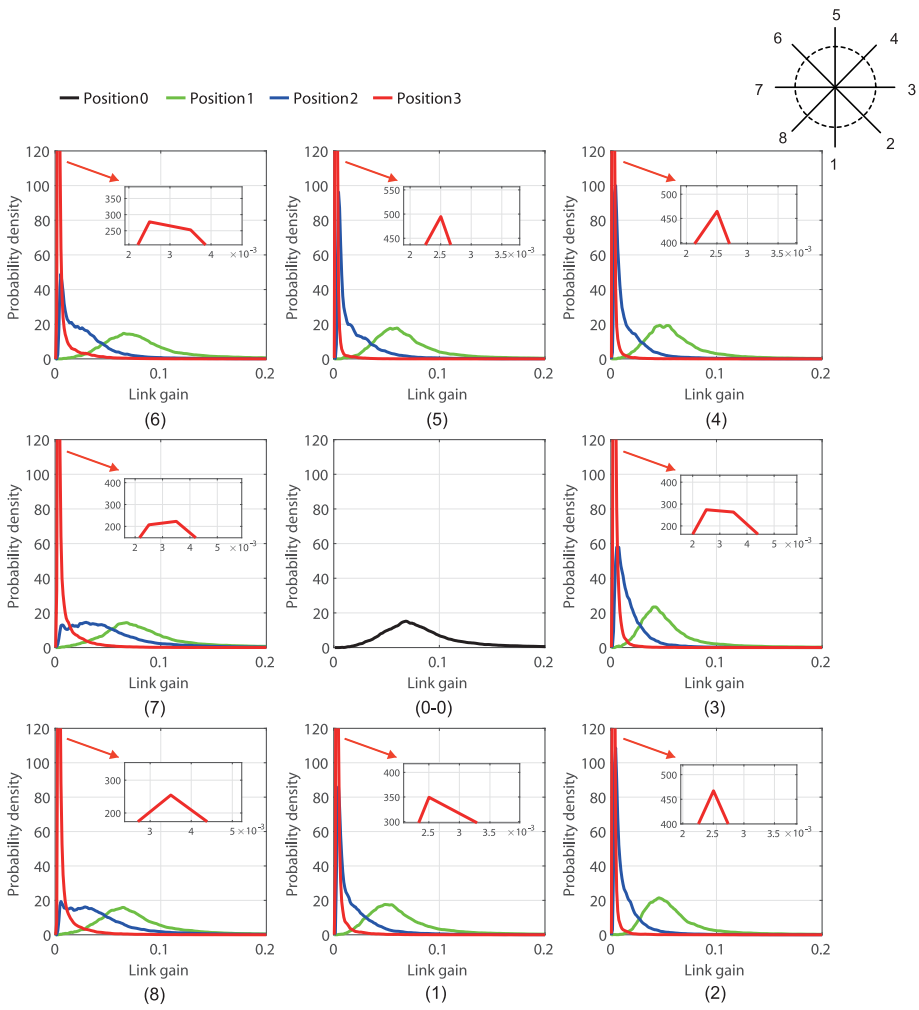

Fig. 10. Probability density of the link gain at each receiver point under wavy surface condition.

(ART Technology USB3103 A, 500 kSPS) and downloaded to a computer for offline analysis. At each position, we have collected data in 300 seconds under calm and wavy surface conditions. The channel link gain can be recovered using Eq. (6). The cutoff frequencies of the low-pass filter and high-pass filter are both 20 kHz.

Note that the experimental water tank's limited space may lead to a reflection of the echo wave superposed to the direct waves. As is one common case in real scenarios, a reflection of the echo wave may also exist, e.g., near the ship in the ocean or near the shore. The coverage characteristics in the presence of echo wave provide significant guidance for communication protocol design and related performance analysis in complicated environments where echo wave cannot be suppressed. It still requires further investigation on the performance comparison in the cases with and without echo wave.

5. Experimental Results

Figure 6 shows the coverage and intensity distribution of light spot under calm and wavy surface conditions. It is observed that under calm surface condition, the shape of the spot is a circle with clear boundary. However, under wavy surface condition, the spot expands or shrinks irregularly in different directions with certain black areas of no optical intensity on the plane. Therefore, the wavy surface can be regarded as a spatial light modulator that changes randomly with time.

Figure 7 shows the original received signal waveforms and extracted link gains at four radial positions in direction 8 (e.g., receiver points 0-0, 8-1, 8-2 and 8-3) under calm surface condition. Based on the typical LED model (e.g., Lambertian model), the light intensity decreases with the LED irradiance angle and the transmission distance. Noting that the LED irradiance angle and the transmission distance at receiver point 8-1 are both larger than those at receiver point 0-0, the link gain at point 0-0 is larger than that at point 8-1. Only part of the APD aperture is within the spot at receiver point 8-2. Since APD aperture is outside the spot at receiver point 8-3, no signal can be received in that condition.

Figure 8 shows the original received signal waveforms and extracted link gains at four radial positions in direction 8 under wavy surface condition. Obviously, at each points, the link gain changes significantly over time during 1 s and the ratio of the maximum to the mean is about ten times. From receiver point 0-0 to receiver point 8-3, the mean link gain gradually decreases under calm surface condition. The fluctuation peak value and frequency of link gains at receiver point 8-2 and receiver point 8-3 are even less pronounced than those at receiver point 0-0. However, at receiver point 8-3, compared with the case in calm surface condition with no signal received at all, APD can still receive the signal under wavy surface due to the refraction on random slope.

The results of link gain extraction method can be verified simply. The upper envelope of the received signal waveform represents the received signal point $y(t)$ when $\sin(2\pi f_c t + \varphi) = 1$, i.e., $r(t) \otimes dh(t) + RAh(t)$. Similarly, the lower envelope of the received signal waveform is $r(t) \otimes dh(t) - RAh(t)$. The link gain $RAh(t)$ at time t is equal to half of the difference of the upper envelope $r(t) \otimes dh(t) + RAh(t)$ and lower envelope $r(t) \otimes dh(t) - RAh(t)$.

We can process the received signals at other receiver points using same method. Some statistics of the link gain are shown in Fig. 9. First, we consider the 17 points inside or on the edge of the light spot (receiver point 0-0 and positions 1 and 2 in eight directions, shown in Fig. 5(b)). Among the 17 points, 6 points have larger mean link gains under wavy surface condition than those under calm surface condition, as highlighted in Fig. 9. Next, we consider the 8 points outside the light spot (position 3 in eight directions). For these 8 points, the mean link gains under calm and wavy surface conditions are both small. However, the maximum link gains under wavy surface condition are likely to be much larger than those under calm surface condition (e.g., 0.0046 versus 0.3702 at receiver point 8-3). It implies that even if APD cannot receive any signal under calm surface condition and the channel quality is poor for a long time, it is possible to receive signals large enough under wavy surface condition, which can fit the setting of opportunistic communication.

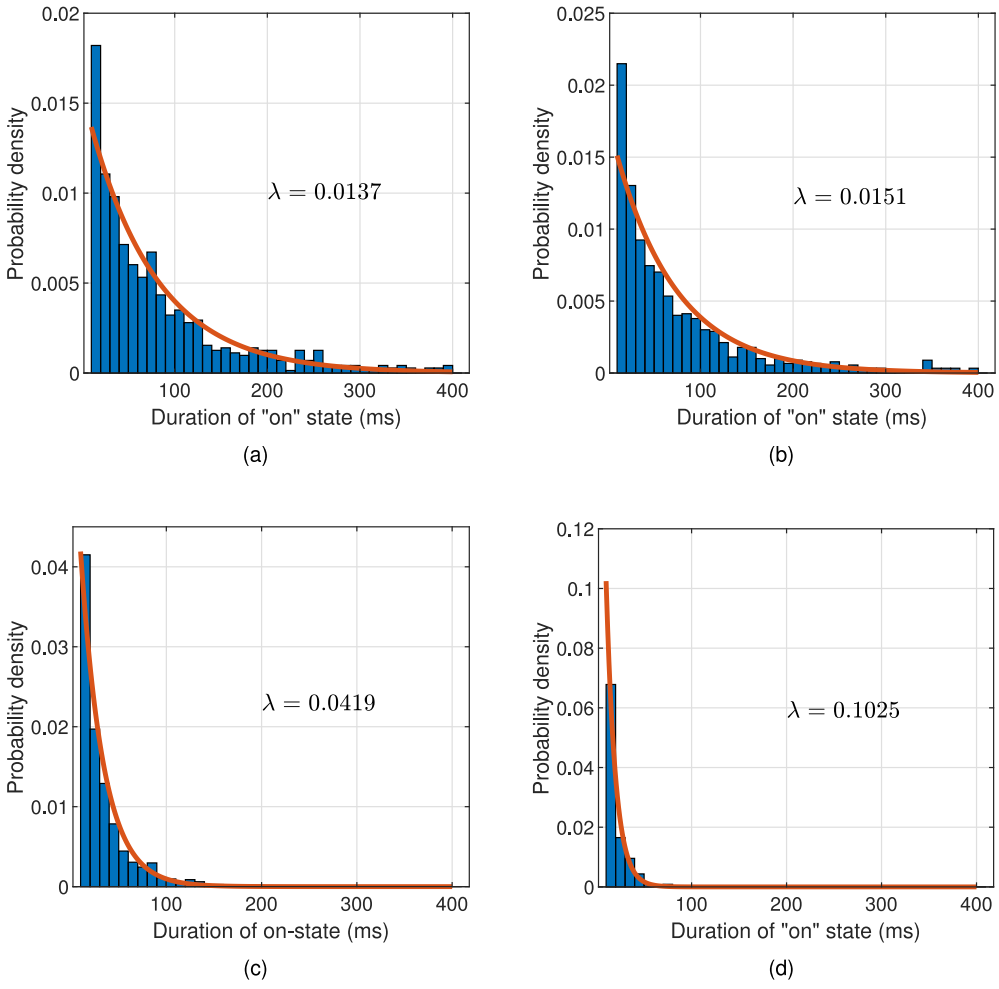

Fig. 11. Probability density of the "on" state duration in direction 8 under wavy surface condition. (a) Receiver point 0-0. (b) Receiver point 8-1. (c) Receiver point 8-2. (d) Receiver point 8-3.

Figure 10 plots the probability densities of the link gains at the receiver points under wavy surface condition. The subfigures are arranged in their actual spatial direction (shown in Fig. 5(b)). The probability densities of link gains are different in different directions. When APD is inside the light spot (0-0 and position 1), the distribution of link gain tends to be right-skewed. A long trailing tail can be observed in the high link gain region, implying a large fluctuation of the link gain. When APD is outside the light spot (position 3), the values of the link gain are mainly concentrated in low region, but it is still likely to reach the large value, especially in 6-3, 7-3, 8-3 (these are in a similar direction). Although the channel is in deep fading for a long time, the beam at the edge of the facula may be deflected by the wavy surface and received. The characteristics of the link gain probability in position 2 lie between positions 1 and 3. At receiver points 1-2, 2-2, 3-2, 4-2, 5-2, the link gain probability is closer to that at position 3 in the corresponding direction, while at receiver point 7-2, the link gain pdf is closer to that at receiver point 7-1. In receiver points 6-2 and 8-2, the link gain probabilities have two peaks. Therefore, the link gain of the position 2 in each direction can be regarded as the transition from position 1 to position 3. In the low link gain region, the channel is similar to that of position 3 — light spot coverage shrinks in such direction and the APD cannot receive any signal. In the high link gain region, the channel is similar to that of position 1 — light spot coverage expands in such direction, and the APD is inside the coverage of light spot.

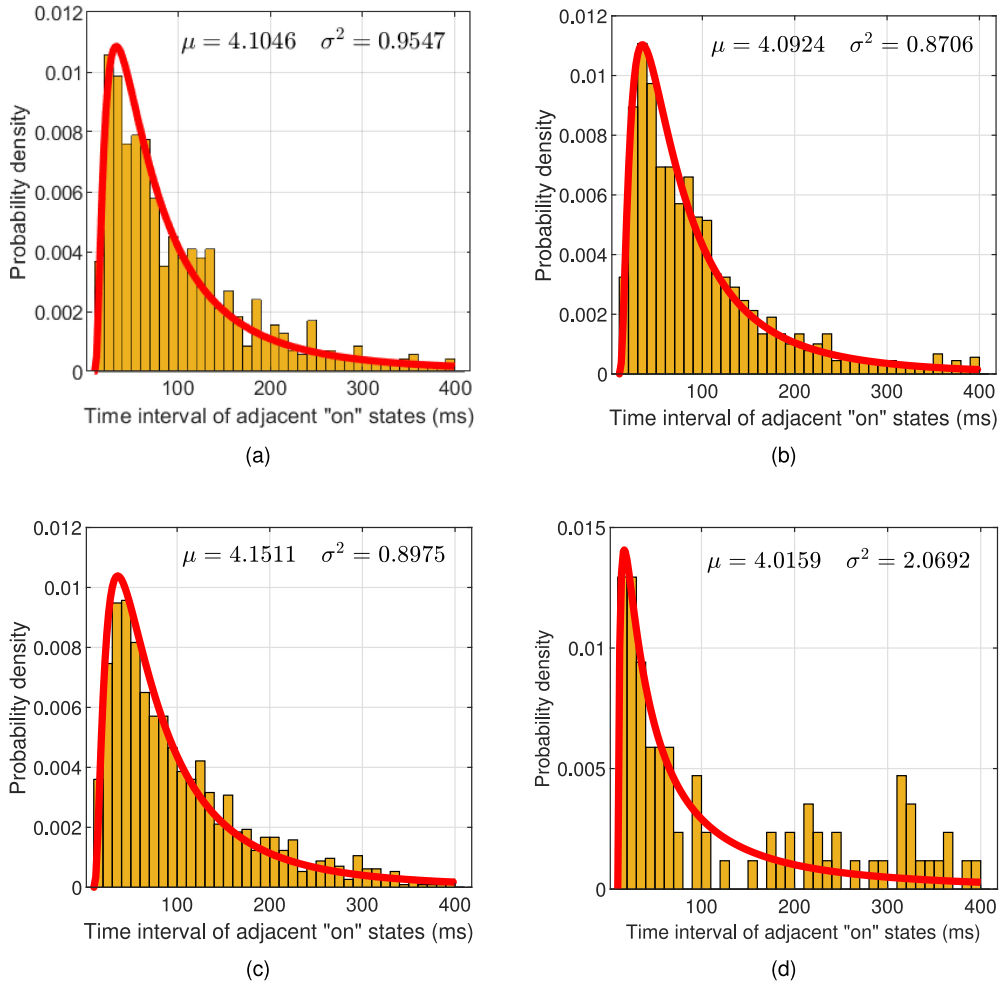

Fig. 12. Probability density of the "on" state interval in direction 8 under wavy surface condition. (a) Receiver point 0-0. (b) Receiver point 8-1. (c) Receiver point 8-2. (d) Receiver point 8-3.

To characterize the event of reliable communication, we set the link gain threshold h_m, and assume that reliable communication can be achieved only when the instantaneous link gain is higher than h_m. In the experiment, threshold h_m can be set as the mean link gain of all receiver points under wavy surface condition. Moreover, to guarantee sufficient time for establishing a communication link, we set the duration threshold of available communication as τ_d, for example, 10 ms, and a communication link is established (or the link is in "on" state) only when the duration of available communication is longer than τ_d.

Figure 11 shows the probability density of the "on" state duration t_d in direction 8 under wavy surface condition. It is seen that the "on" state duration can be well fitted by a shifted exponential distribution with rate parameter λ, i.e.,

$$f_{t_d}(t_d) = \lambda e^{-\lambda(t_d - \tau_d)}, \ t_d \geq \tau_d. \tag{7}$$

Moreover, the mean of "on" state duration (i.e., inverse of the rate parameter λ) decreases with the distance between receiver points and light spot center. This is due to the fact that the receiver point with larger mean link gain is more likely to maintain a reliable communication link. Figure 12 shows the probability density of "on" state interval t_i. It is seen that the "on" state interval can be well fitted

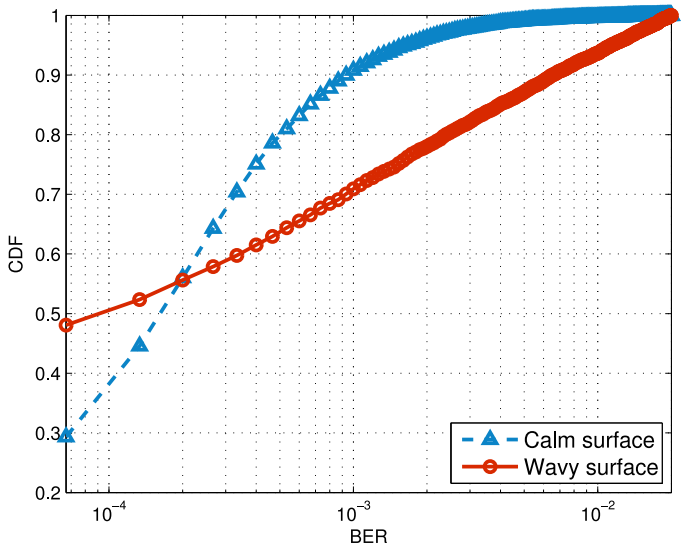

Fig. 13. CDF of BER at receiver point 8-1 under calm and wavy water surface conditions.

by a shifted lognormal distribution with parameters μ and σ, i.e.,

$$f_{t_i}(t_i) = \frac{1}{t_i\sqrt{2\pi\sigma^2}} \exp\left\{-\frac{(\ln(t_i - \tau_d) - \mu)^2}{2\sigma^2}\right\}, \ t_i \geq \tau_d. \tag{8}$$

In Fig. 12(d), there exists some discrepancy between the real probability density of t_i and the fitting curve in the tail region, as communication is unavailable for a long time at position 3.

To evaluate the W2A-VLC transmission performance, we measure the BER at receiver point 8-1 under calm and wavy water surface conditions. On-off keying (OOK) modulation is employed with 10 MHz signal rate and the frame length is 15000. Fig. 13 presents the cumulative distribution function (CDF) of BER at receiver point 8-1 over 300 seconds. It is seen that the probabilities in low BER regime and high BER regime under wavy water surface condition are higher than those under calm water surface condition, which results from the fact that the wavy water surface expands the variation range of link gain.

6. Conclusion

We have investigated the coverage characteristics of W2A-VLC link under calm and wavy water conditions. One effective method has been proposed to extract the variation of channel gain under calm and wavy water surface conditions. By analyzing the real channel gains at different receiver points, it is concluded that the mean channel gain under wavy water surface condition can be larger than that under calm water surface condition, especially when the transmitter and receiver are not perfectly aligned, due to the random spatial modulation effect of wavy water surface. Moreover, the "on" state duration and interval can be well fitted by a shifted exponential distribution and a shifted lognormal distribution, respectively. BER results reveal the effect of expanded link gain variation under wavy water surface condition. Future works include the communication protocol design and related performance analysis based on the coverage characteristics of W2A-VLC link. Besides, further experiments in real scenarios are required to compare W2A links using different optical wavelengths.

Acknowledgment

The authors wish to thank the anonymous reviewers for their valuable suggestions.

References

[1] D. Pompili and I. F. Akyildiz, "Overview of networking protocols for underwater wireless communications," *IEEE Commun. Mag.*, vol. 47, no. 1, pp. 97–102, Jan. 2009.

[2] Z. Zeng, S. Fu, H. Zhang, Y. Dong, and J. Cheng, "A survey of underwater optical wireless communications," *IEEE Commun. Surveys Tuts.*, vol. 19, no. 1, pp. 204–238, 2017.

[3] M. S. Islam, M. Younis, and A. Ahmed, "Communication through air water interface using multiple light sources," in *Proc. IEEE Int. Conf. Commun.*, 2018, pp. 1–6.

[4] M. S. Islam and M. F. Younis, "Analyzing visible light communication through air-water interface," *IEEE Access*, vol. 7, pp. 123830–123845 , 2019.

[5] P. Nabavi and M. Yuksel, "Performance analysis of air-to-water optical wireless communication using SPADs," in *Proc. IEEE Global Commun. Conf.*, 2019, pp. 1–6.

[6] L. Zhang, H. Wang, X. Zhao, F. Lu, X. Zhao, and X. Shao, "Experimental demonstration of a two-path parallel scheme for m-QAM-OFDM transmission through a turbulent-air-water channel in optical wireless communications," *Opt. Exp.*, vol. 27, no. 5, pp. 6672–6688, Mar. 2019.

[7] A. Wang *et al.*, "Adaptive water-air-water data information transfer using orbital angular momentum," *Opt. Exp.*, vol. 26, no. 7, pp. 8669–8678, Apr. 2018.

[8] K. P. Hunt, J. J. Niemeier, and A. Kruger, "RF communications in underwater wireless sensor networks," in *Proc. IEEE Int. Conf. Electro/Infor. Technol.*, 2010, pp. 1–6.

[9] A. Song, M. Stojanovic, and M. Chitre, "Editorial underwater acoustic communications: Where we stand and what is next?," *IEEE J. Ocean. Eng.*, vol. 44, no. 1, pp. 1–6, Jan. 2019.

[10] F. Tonolini and F. Adib, "Networking across boundaries: Enabling wireless communication through the water-air interface," in *Proc. Conf. ACM Special Int. Group Data Commun.*, 2018, pp. 117–131.

[11] Y. Chen *et al.*, "26 m/5.5 gbps air-water optical wireless communication based on an OFDM-modulated 520-nm laser diode," *Opt. Exp.*, vol. 25, no. 13, pp. 14 760–14 765, Jun. 2017.

[12] C.-Y. Li, H.-H. Lu, Y.-C. Huang, Q.-P. Huang, J.-Y. Xie, and S.-E. Tsai, "50 gb/s PAM4 underwater wireless optical communication systems across the water-air-water interface," *Chin. Opt. Lett.*, vol. 17, no. 10, Oct. 2019, Art. no. 100004.

[13] P. Nabavi, A. S. Haq, and M. Yuksel, "Empirical modeling and analysis of water-to-air optical wireless communication channels," in *Proc. IEEE Int. Conf. Commun. Workshops*, 2019, pp. 1–6.

[14] T. Lin, C. Gong, J. Luo, and Z. Xu, "Dynamic optical wireless communication channel characterization through air-water interface," in *Proc. IEEE/CIC Int. Conf. Commun. China*, 2020, pp. 173–178.

[15] A. Wang *et al.*, "Experimental demonstration of a feedback-assisted orbital angular momentum-based underwater wireless optical link across the underwater-to-air interface," in *Proc. 16th Int. Conf. Opt. Commun. Netw.*, 2017, pp. 1–3.

[16] X. Sun, M. Kong, C. Shen, C. H. Kang, T. K. Ng, and B. S. Ooi, "On the realization of across wavy water-air-interface diffuse-line-of-sight communication based on an ultraviolet emitter," *Opt. Exp.*, vol. 27, no. 14, pp. 19635–19649, Jul. 2019.

[17] X. Sun *et al.*, "Field demonstrations of wide-beam optical communications through water-air interface," *IEEE Access*, vol. 8, pp. 160480–160489, 2020.

[18] Y. Shao, R. Deng, J. He, K. Wu, and L.-K. Chen, "Real-time 2.2-Gb/s water-air OFDM-OWC system with low-complexity transmitter-side DSP," *IEEE/OSA J. Lightw. Technol.*, vol. 38, no. 20, pp. 5668–5675, Oct. 2020.

[19] Y. Shao, X. Tang, L. Zhang, R. Jiang, C. Sun, and L.-K. Chen, "On the performance of DCrT-spread-OFDM via water-air OWC system through waves," in *Proc. Opto-Electron. Commun. Conf.*, 2020, pp. 1–3.